Electrochemical properties of Gd(III) ions in LiCl-KCl-$GdCl_3$ at 723–1023 K

Stephanie Castro Baldivieso[1], Nathan D. Smith[1], Zi-Kui Liu[1], Hojong Kim[1*]

[1]Materials Science and Engineering, The Pennsylvania State University, University Park, PA 16802, United States of America

Author E-mail addresses:
szc6095@psu.edu, nds174@psu.edu, zxl15@psu.edu, huk29@psu.edu

Corresponding Author:
*E-mail: huk29@psu.edu. Tel: 814-865-3117. Fax: 814-865-2917

ABSTRACT

Electrochemical behavior of Gd(III) ions in molten LiCl-KCl-$GdCl_3$ was investigated at 723–1023 K via cyclic voltammetry using tungsten as a working electrode, Gd-Bi (mole fraction, x_{Gd} = 0.16) as a reference electrode, and Gd-Bi (x_{Gd} = 0.02) as a counter electrode. A single reduction-oxidation wave was observed, confirming a single-step, 3-electron transfer Gd(III)/Gd transition. The cathodic peak potential exhibited minimal change (< 13 mV) over a wide range of scan rates (0.05–0.30 V s^{-1}), indicating facile charge transfer kinetics (i.e., a reversible electrode process). A nucleation overpotential associated with solid Gd deposition was observable at low temperatures (T < 823 K). The mass transport properties of Gd(III) ions were estimated using the Berzins and Delahay relation based on diffusion-limiting peak current. The diffusivity values were determined to be $D_{Gd(III)}$ = 0.5–2.7×10^{-5} cm^2 s^{-1} at 723–1023 K with an associated activation energy of E_a = 33.9 (±1.0) kJ mol^{-1}. The two-phase [liquid + GdBi] Gd-Bi alloy reference electrode experienced less than 0.5 mV of drift over 5 days of repeated electrochemical measurements, indicating high stability.

Key Words: Gd deposition; Gd(III)/Gd redox couple; diffusivity; two-phase reference electrode

1. INTRODUCTION

The study of electrochemical transitions of rare-earth elements is essential for developing recovery processes that enable recycling for end-of-life products from clean energy technologies such as permanent magnets [1] or used nuclear fuels (UNF) [2]. For instance, in the case of metallic UNF, pyroprocessing recovers uranium in LiCl-KCl-UCl_3 at 773 K via electrorefining for re-use as nuclear fuel in reactors; however, this results in the accumulation of rare-earth fission products in the electrolyte which must be removed via electrodeposition (lanthanide drawdown) to maintain process efficiency [3]. Among rare-earth elements, low recovery efficiency has been reported for Nd, possibly due to its multivalent states in molten chlorides via comproportionation reaction (i.e., $Nd + 2NdCl_3 \rightarrow 3NdCl_2$) and its high reactivity with molten salts [4]. On the other hand, the Gd(III)/Gd transition has been shown to exhibit a single-step deposition process, $Gd(III) + 3e^- \rightarrow Gd$ in molten chlorides (e.g., eutectic LiCl-KCl) [5], promising a higher recovery efficiency and value as a model system for investigating rare-earth recovery processes.

The Gd(III)/Gd transition has been studied using electroanalytical techniques including cyclic voltammetry (CV) and chronopotentiometry (CP) to assess the reversibility of the electrode process and mass transport properties of Gd(III). The single reduction step for Gd(III)/Gd in eutectic LiCl-KCl is agreed upon; however, inconsistent electrode processes have been postulated. Though reversibility has been determined by analyzing the cathodic peak potential as a function of scan rate in all cases, a variety of conclusions have been drawn, including (1) a fully reversible process by Bermejo et al. at 673–823 K [6], (2) a quasi-reversible process by Samin et al. [7], Caravaca et al. at 723–873 K [5], and Tang et al. at 683–813 K [8], and (3) an irreversible process by Shaltry et al. at 773 K [9]. As the reversibility of the electrode process often dictates the analytical methodology, various analytical approaches were

implemented to estimate the mass transport properties of Gd(III); the Berzins-Delahay relation was used for reversible processes from CV data, whereas the Sand equation from CP data, a convolution (semi-integral) technique from CV data, and a simulation technique [5–9] were utilized under assumptions of quasi-reversibility or irreversibility. These differences in analytical approach may have led to the wide range of diffusivity values and activation energies for Gd(III) in eutectic LiCl-KCl.

Inconsistencies in reported Gd(III)/Gd reversibility in previous works may originate in part from differences in electrochemical cell designs. In particular, the use of questionably stable reference electrodes (RE) based on quasi-REs or the Ag/Ag^+ couple may be responsible for the disagreements regarding reversibility. Quasi-REs are known to exhibit drift in potential over time in electrochemical measurements and do not maintain a reproducible reference potential between experiments [10]. A potential drift (~5 mV in 40 h) in the Ag/Ag^+ RE has been observed during electrochemical measurements at low concentrations of AgCl (0.5–2 wt%) between 700–920 K [11], due to the evaporation of reference electrolyte at elevated temperatures which alter the concentration of Ag^+ ions in the electrolyte [11–13]. While a 5 mV drift may seem small, the determination of reversibility often relies on the analysis of cathodic peak potential stability vs. scan rate and any instability in the RE will impact the conclusion. Electrochemical measurements using a Ag/Ag^+ RE will experience increased potential drift over extended periods of cell operation at elevated temperatures.

In addition, the previous studies mostly employed inert glassy C or refractory metals (Mo and W) as the counter electrode (CE) [5–9]. Use of these CE materials should be carefully considered for voltametric studies in molten salts as they will result in consumption $GdCl_3$ in the electrolyte (for glassy C) or contamination of the electrolyte (for refractory metals). During the

reduction of Gd(III), the Cl_2(g) evolution at an inert CE will consume $GdCl_3$ via decomposition ($GdCl_3 \rightarrow Gd(s) + 1.5Cl_2(g)$) or the dissolution of a refractory CE (W or M) will contaminate the electrolyte ($W \rightarrow W^{3+} + 3e^-$). The use of an inert CE (glassy C) is expected to be a better choice but will lead to uncontrolled changes in Gd(III) concentration during repeated voltametric measurements, affecting the current responses and the estimation of diffusivity.

In this work, the electrochemical behavior of Gd(III) in LiCl-KCl-$GdCl_3$ (60.3-38.8-0.9 mol%) is investigated over a wide range of temperatures (723–1023 K) to elucidate the reversibility of the Gd(III)/Gd reaction, employing a unique three-electrode cell comprised of a Gd-Bi alloy (mole fraction, x_{Gd} = 0.02) CE to balance the reaction at the tungsten working electrode (WE), thereby maintaining Gd(III) concentration in the electrolyte, and a stable two-phase Gd-Bi alloy (x_{Gd} = 0.16) as the RE. The use of the Gd-Bi CE will replenish Gd(III) via oxidation instead of Cl_2 evolution from an inert CE, and the two-phase Gd-Bi reference electrode has been shown to vary by less than 2 mV over the course of more than 20 days of operation [14], indicating significantly improved stability over quasi-REs and the Ag/Ag^+ RE. The two-phase Gd-Bi RE was calibrated vs. pure Gd by Baldivieso et al. [15] and the long-term stability was then demonstrated by Smith et al. [14], which established the electrode's improved stability. Within the operating temperature range, the RE possesses two equilibrium phases (liquid + GdBi) which can maintain a constant redox potential irrespective of compositional uncertainty [14,15]. Cyclic voltammetry was conducted at various scan rates (0.05–0.30 V s^{-1}) to determine characteristic signals of peak potential, peak current, potential at zero current, and overpotential during Gd deposition. The results at each temperature were analyzed to assess the reversibility of Gd(III)/Gd electrode process, the mass transport properties of Gd(III), and were compared to results from previous works.

2. EXPERIMENTAL SECTION

2.1 Electrochemical cell components

The electrochemical cell components were prepared and assembled in an argon-filled glovebox (< 0.5 ppm O_2, < 0.5 ppm H_2O) due to the hygroscopic nature of chloride salts and the high oxygen affinity of Gd-Bi alloys.

Electrolyte: The LiCl-KCl-$GdCl_3$ electrolyte (60.3-38.8-0.9 mol%) was prepared by weighing appropriate amounts of LiCl (Ultra Dry, 99.9%, Alfa Aesar), KCl (Ultra Dry, 99.9%, Alfa Aesar), and $GdCl_3$ (anhydrous, 99.9%, Alfa Aesar). The electrolyte mixture (~65 g) was loaded into a quartz crucible (Technical Glass Products) for pre-melting inside a stainless-steel vacuum chamber. The chamber was evacuated (< 10 mtorr) and heated to 373 K for 12 h and then at 543 K for 12 h to remove residual moisture. The chamber was then purged with high-purity argon gas three times and heated to 973 K under flowing argon for 3 h to homogenize the electrolyte. The electrolyte was cooled to room temperature and crushed into a fine powder with a mortar and pestle in the glovebox environment. The composition of the electrolyte was analyzed using inductively coupled plasma atomic emission spectroscopy (ICP-AES Perkin-Elmer Optima 5300DV) with a maximum error of 4% of the measured value.

Electrodes: The working electrode was prepared using a tungsten wire (1 mm diameter, 40.6 cm length; 99.95%, Thermo Shield) for electrochemical measurements by polishing the surface up to 100 grit using SiC paper and cleaning with isopropanol. The Gd-Bi alloys (x_{Gd} = 0.02 and 0.16) were fabricated with an arc melter (Edmund Bühler, MAM-1) using 1.51 and 12.54 wt.% of pure Gd (99.9%, Alfa Aesar) and 98.49 and 87.46 wt.% of Bi (99.9%, Sigma Aldrich) metal pieces, respectively. The reference electrode was prepared by melting ~2.5 g of Gd-Bi alloy (x_{Gd} = 0.16) in a boron nitride (BN) crucible (8 mm inner diameter, 12 mm outer

diameter, 15 mm depth, and 20 mm height; AdValue Technology) using an induction heater (IH15A-2T, Across International) custom installed in the glove box. During induction melting of the Gd-Bi alloy, a tungsten electrical lead wire (1 mm diameter) was inserted into the molten alloy to establish electrical contact. The counter electrode was prepared in a similar manner as described for the RE, using ~16 g of Gd-Bi alloy (x_{Gd} = 0.02) in a larger BN crucible (21 mm inner diameter, 25 mm outer diameter, 20 mm depth, and 22 mm height; AdValue Technology).

Electrochemical cell assembly: The electrodes were arranged inside an alumina crucible (60 mm diameter, 100 mm height; AdValue Technology) and ~65 g of homogeneous electrolyte powder was poured into the crucible. The schematic of the three-electrode cell configuration is presented in Figure 1. The W electrical leads were inserted into alumina tubes, sealed at the top with epoxy, and the electrochemical cell assembly was placed into a stainless-steel chamber. The chamber was sealed inside the glovebox and loaded into a crucible furnace (Mellen Company). The assembled electrochemical cell was dried following the same procedure described for preparing the electrolyte. The chamber was purged with high-purity argon three times, and then heated to 873 K under flowing argon (10 mL min^{-1}).

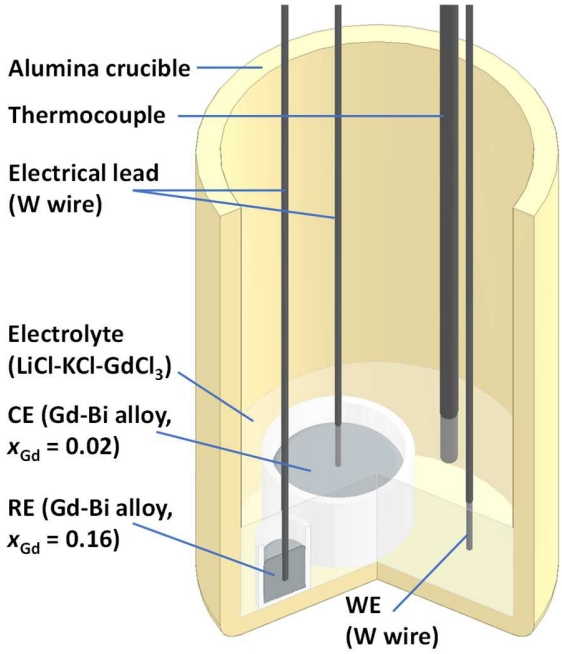

Figure 1. Schematic of three-electrode cell employed for electrochemical measurements of Gd(III) in LiCl-KCl-$GdCl_3$ (60.3-38.8-0.9 mol%) electrolyte at 723–1023 K.

2.2 Electrochemical measurements

Electrochemical measurements were performed using a potentiostat-galvanostat (Autolab PGSTAT302N, Metrohm AG) and cell temperatures were recorded using a thermocouple (ASTM Type K) and data acquisition system (NI 9211, National Instruments). The cell temperature was heated/cooled between 723 and 1023 K in 25 K increments at a rate of 5 K min^{-1}. At each increment, the cell temperature was held constant for ~1.5 h to reach thermal steady state before electrochemical measurements were initiated. At each temperature, cyclic voltammetry was conducted three times at scan rates from 0.05 up to 0.30 V s^{-1} and electrochemical impedance spectroscopy was performed (EIS) over a frequency range of 10–10^5 Hz with an amplitude of 0.010 V. The voltammograms were *IR*-corrected using the uncompensated solution resistance (R_u) determined from EIS measurements (high frequency

intercept). The nominal surface area (A) of the WE was determined to be $A = 0.134$ cm^2 based on the immersion depth of the tungsten wire in the salt after cooling the cell.

3. RESULTS AND DISCUSSION

Electrochemical properties of Gd(III) in eutectic LiCl-KCl were investigated via cyclic voltammetry at 723–1023 K (Figure 2). A single reduction-oxidation wave was consistently observed at all temperatures, suggesting a single-step, 3-electron transfer reaction [Gd(III) + $3e^-$ = Gd(s)] in the chloride salt. During the forward sweep, a clear cathodic peak current ($I_{p,c}$) and potential ($E_{p,c}$) were observed (Figure 2a). During the reverse sweep, the potential at zero current (E_{cell}) was marked where the current flow crosses from the cathodic to anodic direction, which can be approximated as Gd(III)/Gd redox potential for calibrating the Gd-Bi ($x_{Gd} = 0.16$) RE. The characteristic potentials (E_{cell}, $E_{p,c}$) and currents ($I_{p,c}$) were analyzed as a function of temperature to assess the reliability of the E_{cell} value for the RE calibration, the reversibility of the Gd(III)/Gd electrode process, and the mass transport properties of Gd(III) ions. The anodic peak potentials and currents were not considered for these analyses as the limiting behavior during oxidation can originate from complete depletion and consumption of deposited Gd from the WE surface, as opposed to the mass transport limit of Gd(III) near the electrode-electrolyte interface.

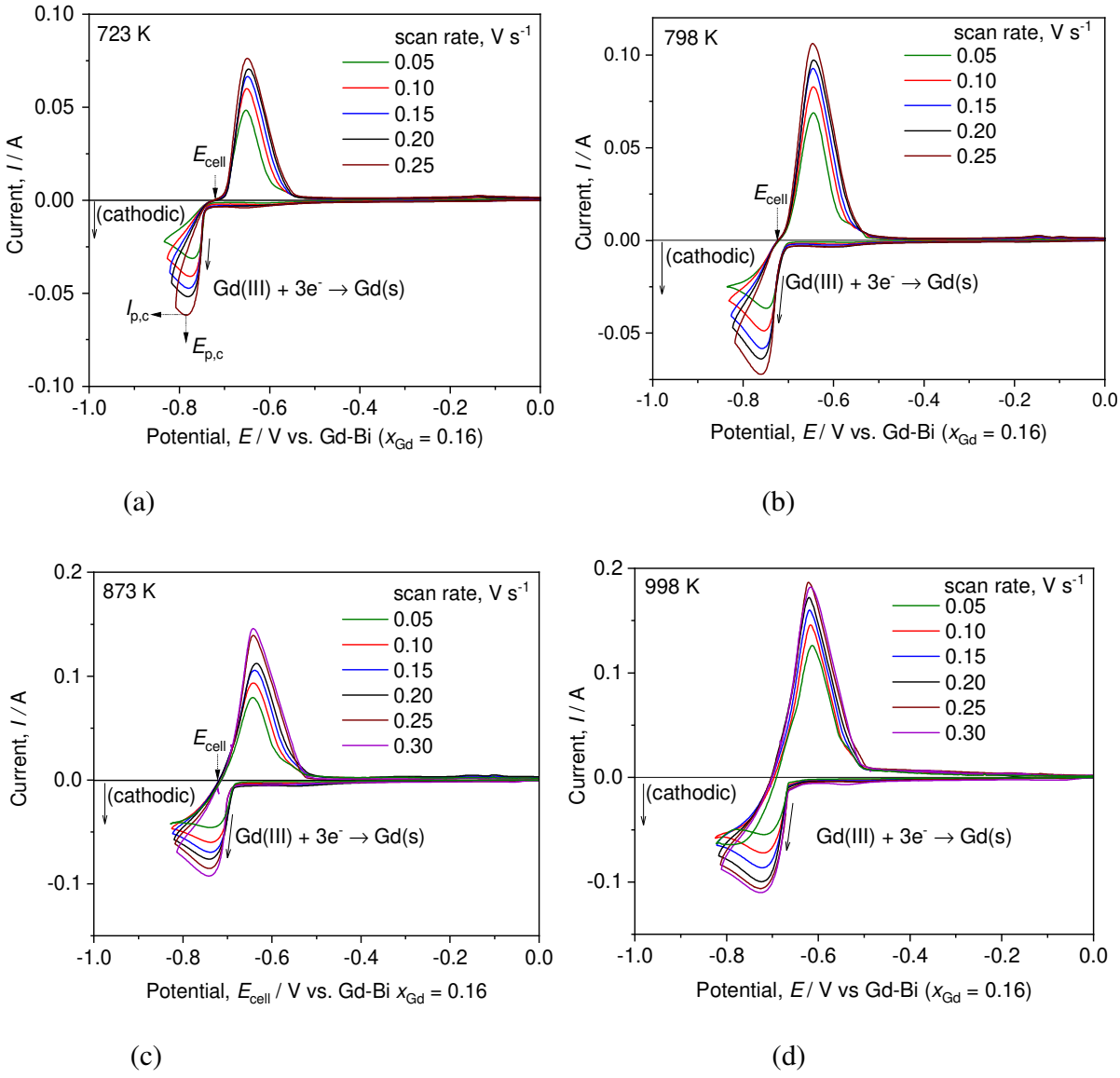

Figure 2. Cyclic voltammograms using tungsten WE vs. Gd-Bi (x_{Gd} = 0.16) in LiCl-KCl-$GdCl_3$ (60.3-38.8-0.9 mol%) electrolyte at scan rates from 0.05 up to 0.30 V s^{-1} at (a) 723 K, (b) 798 K, (c) 873 K and (d) 998 K. All voltammograms were *IR*-corrected using uncompensated solution resistance (R_u) from EIS measurements.

3.1 Calibration of the Gd-Bi (x_{Gd} = 0.16) alloy versus pure Gd

The potential at zero current (E_{cell}) during the reverse sweep deviated by less than 10 mV over various scan rates (0.05–0.30 V s^{-1}) at each temperature (Figure 2), and the average E_{cell} is

plotted using data acquired from 13 different temperatures between 723–1023 K (Figure 3). The E_{cell}-T trend from CV measurements was curvilinear, deviating from the linear emf-T trend determined by the authors in the previous work using the following electrochemical cell [15]:

$$\underline{\text{Gd-Bi } (x_{Gd} = 0.16)} \,|\, \text{LiCl-KCl-GdCl}_3 \,|\, \text{Gd(s)} \quad (1)$$

$$emf = \frac{RT}{3F} \ln a^*_{\text{Gd(in Bi)}} \quad (2)$$

where emf is the redox potential of Gd(s) relative to the Gd-Bi alloy (x_{Gd} = 0.16), R is the universal gas constant, T is the temperature in Kelvin, F is the Faraday constant, and $a^*_{\text{Gd(in Bi)}}$ is the activity of Gd in Bi at x_{Gd} = 0.16.

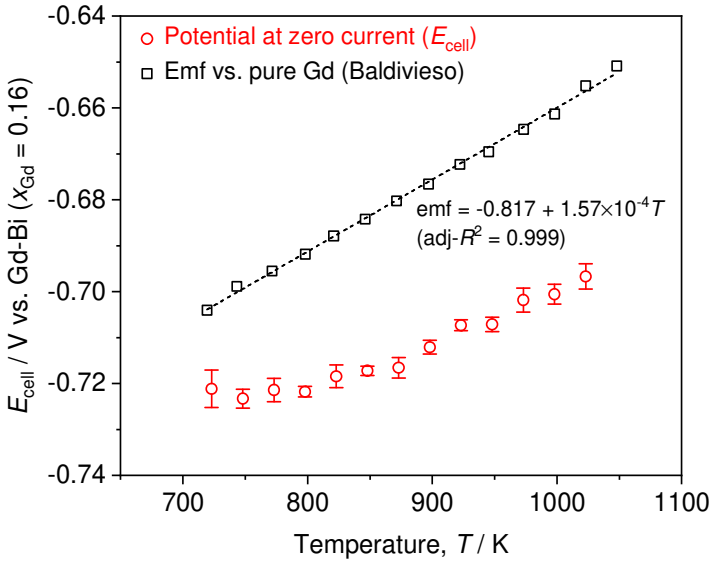

Figure 3. Potential at zero current (E_{cell}) vs. Gd-Bi (x_{Gd} = 0.16) during the reversal sweep in CV measurements (Figure 2) at 723–1023 K, compared to the emf values of Gd(s) vs. Gd-Bi (x_{Gd} = 0.16) using an electrochemical cell of $\underline{\text{Gd-Bi}(x_{Gd} = 0.16)}$|LiCl-KCl-GdCl$_3$|Gd(s) by Baldivieso et al. [15].

The E_{cell} values were consistently more negative than emf values by ~17–50 mV at 723–1023 K with a larger deviation observed at higher temperatures, calling into question the CV-based calibration E_{cell} determination method, which is widely employed in electrochemical

studies to calibrate a RE (e.g., Ag/Ag^+) or quasi-RE [16,17]. The difference between E_{cell} and emf is thought to originate from the depletion of Gd(III) near the electrode surface during potential sweep, shifting E_{cell} due to a concentration polarization effect (E_{conc}) in the negative direction according to:

$$E_{\text{cell}} = \frac{RT}{3F}\ln\frac{a^{*}_{\text{Gd(in Bi)}}a^{\text{s}}_{\text{Gd(III)}}}{a^{\text{b}}_{\text{Gd(III)}}} = emf + \frac{RT}{3F}\ln\frac{a^{\text{s}}_{\text{Gd(III)}}}{a^{\text{b}}_{\text{Gd(III)}}} = emf + E_{\text{conc}} \qquad (3)$$

where $a^{\text{s}}_{\text{Gd(III)}}$ is the activity of Gd(III) near the WE surface and $a^{\text{b}}_{\text{Gd(III)}}$ is the activity of Gd(III) in the bulk electrolyte.

By calibrating the redox potential of Gd-Bi (x_{Gd} = 0.16) RE relative to pure Gd from emf data in Figure 3, the forward sweep data is plotted at 723 K, 873 K, and 998 K at the scan rate of 0.10 V s^{-1} (Figure 4). At 873 K and 998 K, the onset of Gd deposition occurs at ~0.00 V vs. pure Gd with little overpotential, suggesting facile charge transfer kinetics (i.e., reversible electrode process) for the Gd(III)/Gd transition. In contrast, the onset of Gd deposition at 723 K occurs at –0.03 V vs. pure Gd, implying a substantial negative overpotential. A similar negative overpotential was also reported by Bermejo et al. with an observable current loop in the CV waveform at 723 K in LiCl-KCl-$GdCl_3$, indicative of nucleation overpotential from the formation of solid Gd on the WE surface (Figure 2a) [6]. It is noted that the nucleation overpotential at 723 K is distinct from sluggish charge transfer kinetics at the electrode-electrolyte interface that governs the reversibility of electrode processes.

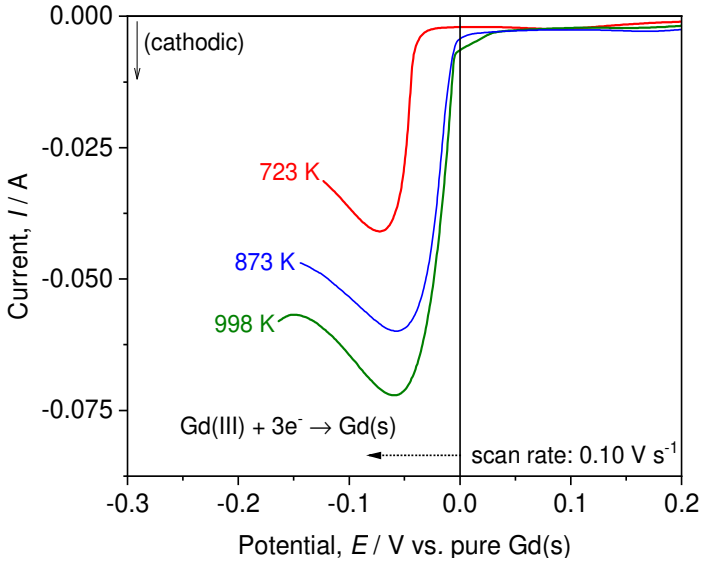

Figure 4. Selected forward sweep of tungsten WE from Figure 2 vs. pure Gd(s) in LiCl-KCl-$GdCl_3$ electrolyte at 723 K, 873 K, and 998 K at the scan rate of 0.10 V s^{-1}, corrected using emf data from ref. [14] in Figure 3.

3.2 Analysis of peak potential and electrode process

The Gd(III)/Gd electrode process was examined using the cathodic peak potential ($E_{p,c}$) determined from the first derivative of the voltammogram by plotting $E_{p,c}$ as a function of scan rate (v) at each temperature (Figure 5). The variation of $E_{p,c}$ was about 6–13 mV over various scan rates (0.05–0.30 V s^{-1}) at all temperatures. Based on the small variation in $E_{p,c}$ as a function of scan rate and minimal charge-transfer overpotential for the onset of Gd deposition, the Gd(III)/Gd transition is assumed to be a reversible electrode process.

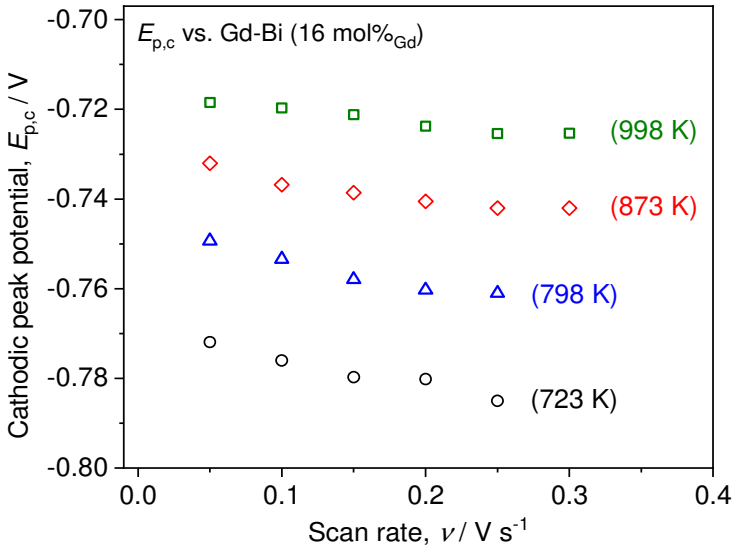

Figure 5. Cathodic peak potential ($E_{p,c}$) vs. Gd-Bi (x_{Gd} = 0.16) from CV data (Figure 2) as a function of scan rate (v) from 0.05 up to 0.30 V s^{-1} at 723–1023 K in LiCl-KCl-$GdCl_3$ electrolyte.

A number of studies on the Gd(III)/Gd transition reported inconsistent electrode processes in eutectic LiCl-KCl electrolyte based on scan rate-dependent variation in $E_{p,c}$ ($\Delta E_{p,c}$), including (1) irreversible process by Shaltry et al. ($\Delta E_{p,c}$ > 30 mV) at 773 K [9], (2) quasi-reversible process by Samin et al. [7] and Caravaca et al. at 723–873 K [5], and (3) reversible process by Bermejo et al. at 673–823 K [6] and this work ($\Delta E_{p,c}$ < 13 mV) at 723–1023 K. The observation of relatively small $\Delta E_{p,c}$ in this work is thought to come from our unique three-electrode cell utilizing Gd-Bi (x_{Gd} = 0.16) as the RE and Gd-Bi (x_{Gd} = 0.02) as the CE (Figure 1) compared to the three-electrode cell configurations used in other works on Gd systems (Table 1). Compared to Ag/Ag^+, or quasi-REs in other works [9,10], the Gd-Bi (x_{Gd} = 0.16) RE maintained an exceptional stability within 0.5 mV (Figure 6) throughout the measurement (~5 days), leveraging the two-phase (liquid + GdBi) stability of the Gd-Bi alloy for maintaining a constant redox potential over a wide range of compositions (Gibbs phase rule). In addition, the reaction at

the CE with the liquid Gd-Bi (x_{Gd} = 0.02) alloy balances the reaction at the WE, maintaining a constant concentration of Gd(III) ($C_{Gd(III)}$) in the electrolyte, in contrast to conventional CEs (W, Mo, or glassy carbon) [6,9], which can result in changes in $C_{Gd(III)}$ over repeated electrochemical measurements.

Table 1. Comparison of three-electrode configuration in this work and previous works in the literature.

	RE	CE	WE
This work	Gd-Bi (x_{Gd} = 0.16)	Gd-Bi (x_{Gd} = 0.02)	W
Caravaca et al. [5]	Ag/AgCl	Mo or glassy carbon	W
Iizuka [18]	Ag/AgCl	Gd	W
Samin et al. [7]	Ag/AgCl	W	W
Tang et al. [8]	Ag/AgCl	Mo	Graphite
Bermejo et al. [6]	Ag/AgCl	W	W
Lantelme et al. [19]	Cl_2 electrode	Gd	W
Shaltry et al. [9]	GC (quasi-RE)	W	W

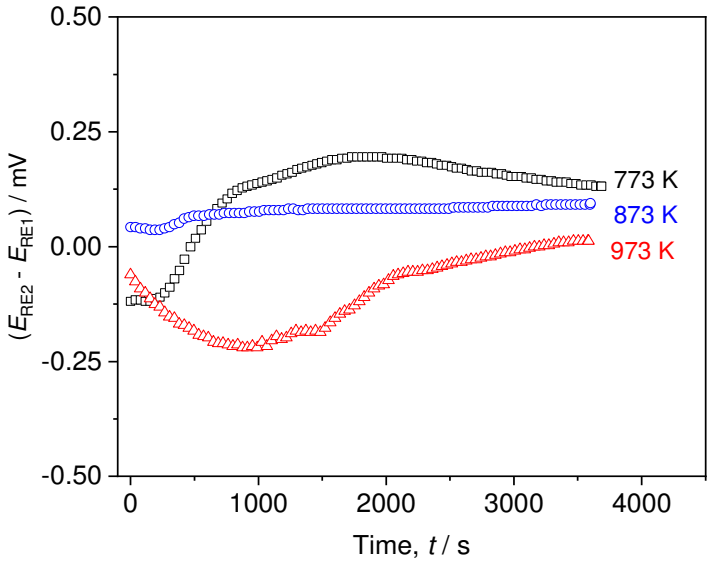

Figure 6. Potential difference between two Gd-Bi alloy (x_{Gd} = 0.16) reference electrodes (E_{RE2} – E_{RE1}) as a function of time in LiCl-KCl-$GdCl_3$ electrolyte at 773–973 K.

3.3 Mass transport properties of Gd(III) ions

The cathodic peak current ($i_{p,c}$) was proportional to the square root of the scan rate ($v^{1/2}$), indicating that the Gd(III)/Gd reaction is under diffusion control at each temperature (Figure 7). The $i_{p,c}$ and its slope increased with temperature due to enhanced mass transport at higher temperatures. Based on the facile charge transfer kinetics for the Gd(III)/Gd couple, this linear relationship was used to estimate the diffusivity ($D_{Gd(III)}$) of Gd(III) ions using the following relation, developed by Berzins and Delahay for reversible and soluble-insoluble electrode processes under the assumption of semi-infinite linear diffusion [20]:

$$i_{p,c} = -0.61AC_{Gd(III)}\left(\frac{n^3F^3D_{Gd(III)}}{RT}v\right)^{\frac{1}{2}} \quad (4)$$

where A is the electrode surface area (A = 0.134 cm^2), $C_{Gd(III)}$ is the molar concentration (mol cm^{-3}), $D_{Gd(III)}$ is the diffusivity of Gd(III) in the electrolyte, and v is the scan rate. The linear diffusion approximation is assumed to hold for a cylindrical electrode as a first approximation, given the fast scan rates employed (> 0.05 V s^{-1}) and rapid mass transport in liquid state [21]. Although the cathodic peak current was proportional to the square root of scan rate, the y-intercept does not directly pass through the origin, possibly due to uncertainties arising from residual currents as a result of non-linear diffusion behavior at the cylindrical electrode, double-layer charging, and challenges in experimental controls at high temperatures. The $C_{Gd(III)}$ was estimated using the density of LiCl-KCl-$GdCl_3$ assuming an ideal mixture of eutectic LiCl-KCl [22] and liquid $GdCl_3$ [23] at each temperature (Table 2).

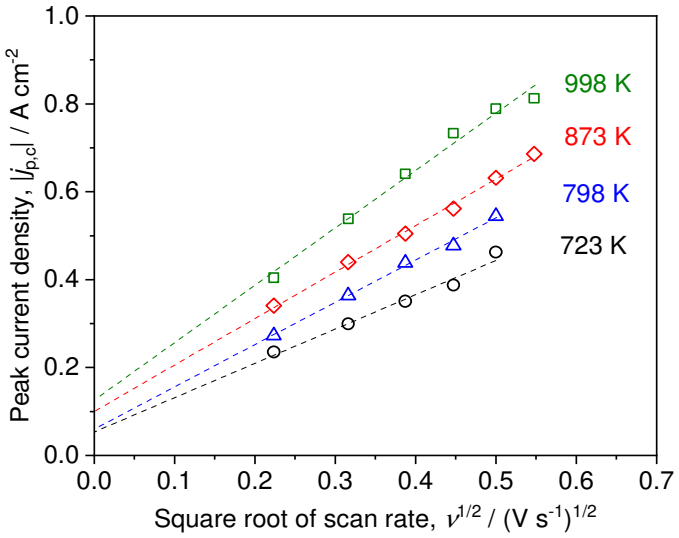

Figure 7. Cathodic peak current density ($j_{p,c}$) as a function of square root of scan rate ($\nu^{1/2}$) at 723–1023 K in LiCl-KCl-$GdCl_3$ from CV data (Figure 2), with nominal electrode surface area: A = 0.134 cm^2. The dashed line represents linear fit at each temperature.

Table 2. Molar concentration ($C_{Gd(III)}$) and diffusivity ($D_{Gd(III)}$) of Gd(III) ions in molten LiCl-KCl-$GdCl_3$ (60.3-38.8-0.9 mol%) electrolyte. The density of the electrolyte ($\rho_{LiCl\text{-}KCl\text{-}GdCl_3}$) was approximated from the densities of eutectic LiCl-KCl ($\rho_{LiCl\text{-}KCl}$) and liquid $GdCl_3$ (ρ_{GdCl_3}) as an ideal mixture at each temperature.

		T				
	Unit	723 K	773 K	823 K	873 K	973 K
$\rho_{LiCl\text{-}KCl}$ †	g cm^{-3}	1.65	1.62	1.60	1.57	1.52
ρ_{GdCl_3} ‡		3.67	3.63	3.60	3.57	3.50
$\rho_{LiCl\text{-}KCl\text{-}GdCl_3}$		1.69	1.66	1.63	1.61	1.55
$C_{Gd(III)}$	mol cm^{-3} (×10^{-4})	2.74	2.70	2.65	2.61	2.52
$D_{Gd(III)}$	cm^2 s^{-1} (×10^{-5})	0.55	0.69	0.95	1.31	2.17

† $\rho_{LiCl\text{-}KCl}(T) = 2.0286 - 5.267 \times 10^{-4} T$ [22]

‡ $\rho_{GdCl_3}(T) = 3.56 - 6.71 \times 10^{-4}(T - 882)$ [23]

The diffusivity of Gd(III) from Eq. (4) is presented as a function of inverse temperature (Figure 8), following Arrhenius behavior with linear $\log(D_{Gd(III)})$-$1/T$ trend. The error values

were estimated from the standard deviation of the slope of $i_{p,c}$ vs. $v^{1/2}$ plot at each temperature. The diffusivity values were ~0.5–2.7×10^{-5} cm^2 s^{-1} at 723–1023 K and the activation energy (E_a) was estimated at E_a = 33.9 (±1.0) kJ mol^{-1} according to:

$$D_{Gd(III)} = D_0 \exp\left(-\frac{E_a}{RT}\right) \quad (5)$$

where D_0 is pre-exponential constant, summarized in Table 3.

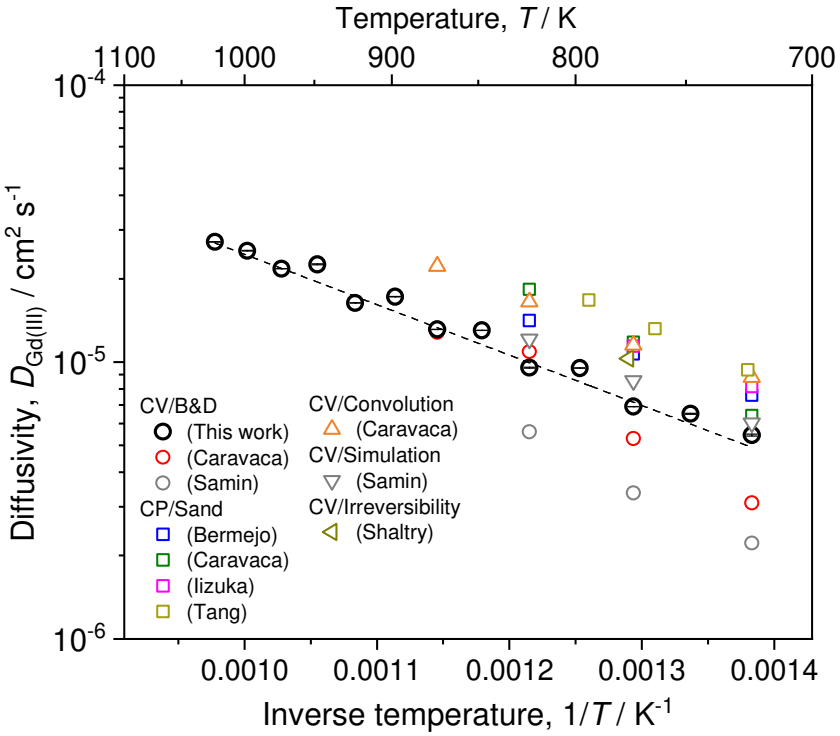

Figure 8. Diffusivity of Gd(III) as a function of inverse temperature (1/T) at 723–1023 K, compared to the reported values in the literature using electrochemical techniques of cyclic voltammetry (CV) and chronopotentiometry (CP) [5–9,18] Note: B&D (Berzins & Delahay), Sand (Sand equation).

Table 3. Comparison of fit parameters (D_0 and E_a) for $D_{Gd(III)}$ in LiCl-KCl-$GdCl_3$ electrolyte according to $D_{Gd(III)} = D_0 \exp\left(-\frac{E_a}{RT}\right)$.

	D_0 / cm^2 s^{-1}	E_a / kJ mol^{-1}	method
This work	1.50×10^{-3}	33.9(±1.0)	CV (Berzins & Delahay)
Caravaca et al. [5]	1.99×10^{-2}	53.38	CV (Berzins & Delahay)
Samin et al. [7]	6.20×10^{-3}	48.1(±4.5)	CV (Berzins & Delahay)
Bermejo et al. [6]	1.62×10^{-3}	32.17	CP (Sand equation)
Iizuka et al. [18]	1.66×10^{-3}	31.96	CP (Sand equation)
Lantelme et al. [19]	1.79×10^{-3}	33.03	CP (Sand equation)
Tang et al.[8]	1.24×10^{-2}	42.80(±1.4)	CP (Sand equation)
Caravaca et al. [5]	1.99×10^{-3}	32.45	CV (convolution)
Samin et al. [7]	1.80×10^{-3}	34.3	CV (simulation)

Overall, the temperature-dependent $D_{Gd(III)}$ values were in close agreement with the previous works using chronopotentiometry via the Sand equation independent of reversibility and the CV-based techniques employing sophisticated mathematical models for quasi-reversible processes [24]. The use of the Berzins-Delahay relation (Eq. (4)) by Caravaca et al. [5] and Samin et al. [7] resulted in inconsistent $D_{Gd(III)}$ and E_a values (Table 3) and the authors attributed this discrepancy to a high degree of quasi-reversibility observed in their CV measurements. However, the consistent results of $D_{Gd(III)}$ and E_a in this work corroborate the reversibility of the Gd(III)/Gd transition and the applicability of the Berzins-Delahay relation for estimating $D_{Gd(III)}$, enabled by a highly reliable electrochemical cell that leverages a stable RE (two-phase Gd-Bi alloy at x_{Gd} = 0.16) and balanced CE (Gd-Bi at x_{Gd} = 0.02).

4. CONCLUSION

The electrochemical properties of Gd(III)/Gd were investigated in molten LiCl-KCl-$GdCl_3$ electrolyte over a wide temperature range between 723–1023 K. A novel cell design was employed using a stable two-phase Gd-Bi (x_{Gd} = 0.16) as the reference electrode (RE) and liquid Gd-Bi (x_{Gd} = 0.02) as the counter electrode (CE). The two-phase Gd-Bi reference electrode

enabled accurate electrochemical property measurements for determining reversibility of the Gd(III)/Gd transition and characteristic potentials by limiting drift in the reference potential less than 0.5 mV over 5 days. The use of liquid Gd-Bi CE balanced the reactions at the WE, maintaining a constant Gd(III) concentration in the electrolyte over repeated electrochemical measurements. Diffusivity values were determined to be $D_{Gd(III)}$ = 0.5–2.7×10^{-5} cm^2 s^{-1} at 723–1023 K using the Berzins and Delahay relation with an activation energy of E_a = 33.9 (±1.0) kJ mol^{-1}. The electrochemical cell design based on the two-phase RE and balanced CE in this work will allow for accurate electrochemical property measurements of rare-earth elements in molten halide electrolytes.

FUNDING

US National Science Foundation. US Department of Energy, Office of Nuclear Energy

CREDIT AUTHORSHIP CONTRIBUTION STATEMENT

Stephanie Castro Baldivieso: Conceptualization, Methodology, Investigation, Writing. **Nathan D. Smith**: Writing–review & editing. **Zi-Kui Liu**: Writing–review. **Hojong Kim**: Writing–review & editing.

DECLARATION OF COMPETING INTEREST

The authors declare they have no known competing financial interests or personal relationship that could have appeared to influence the work reported in this paper.

ACKNOWLEDGEMENTS

This work was supported by the US National Science Foundation (grant No. CBET-1844170) and the US Department of Energy, Office of Nuclear Energy's Nuclear Energy University Programs (Award No. DE-NE0008757) and Integrated University Program Graduate Fellowship (Award No. DE-NE0000113). The authors thank Jarrod Gesualdi for technical assistance in

preparing electrochemical cell components and Michael Shaltry at Idaho National Laboratory for relevant discussions on paper content.

5. REFERENCES

[1] G. Bailey, N. Mancheri, K. Van Acker, Sustainability of Permanent Rare Earth Magnet Motors in (H)EV Industry, Journal of Sustainable Metallurgy. 3 (2017) 611–626. https://doi.org/10.1007/s40831-017-0118-4.

[2] B. Kersten, K. Hawthorne, M. Williamson, R. Akolkar, C.E. Duval, The Future of Nuclear Energy: Electrochemical Reprocessing of Fuel Takes Center Stage, Electrochem Soc Interface. (2021). www.electrochem.org.

[3] M.A. Williamson, J.L. Willit, Pyroprocessing flowsheets for recycling used nuclear fuel, Nuclear Engineering and Technology. 43 (2011) 329–334. https://doi.org/10.5516/NET.2011.43.4.329.

[4] F.J. Keneshea, D. Cubicciotti, Lanthanum-lanthanum trichloride phase diagram, J Chem Eng Data. 6 (1961) 507–509. https://doi.org/10.1021/je60011a008.

[5] C. Caravaca, G. de Córdoba, M.J. Tomás, M. Rosado, Electrochemical behaviour of gadolinium ion in molten LiCl-KCl eutectic, Journal of Nuclear Materials. 360 (2007) 25–31. https://doi.org/10.1016/j.jnucmat.2006.08.009.

[6] M.R. Bermejo, J. Gómez, J. Medina, A.M. Martínez, Y. Castrillejo, The electrochemistry of gadolinium in the eutectic LiCl-KCl on W and Al electrodes, Journal of Electroanalytical Chemistry. 588 (2006) 253–266. https://doi.org/10.1016/j.jelechem.2005.12.031.

[7] A. Samin, E. Wu, J. Zhang, The thermodynamic and transport properties of $GdCl_3$ in molten eutectic LiCl-KCl derived from the analysis of cyclic voltammetry signals, J Appl Phys. 121 (2017). https://doi.org/10.1063/1.4976570.

[8] H. Tang, B. Pesic, Electrochemistry and Electrocrystallization of Gadolinium on Mo Substrate in LiCl–KCl Eutectic Salts, J Electrochem Soc. 161 (2014) D429–D436. https://doi.org/10.1149/2.0371409jes.

[9] M.R. Shaltry, P.K. Tripathy, T.S. Yoo, G.L. Fredrickson, Electrochemical measurement and analysis of YCl_3, $ScCl_3$, $GdCl_3$ and $MgCl_2$ in molten eutectic LiCl-KCl, Journal of Electroanalytical Chemistry. 899 (2021). https://doi.org/10.1016/j.jelechem.2021.115689.

[10] D. Killinger, S. Phongikaroon, Investigation of W, Ag, and Pt Quasi-Reference Electrode Stability in Molten NaCl-$CaCl_2$ with Ce(0)/Ce(III) as an Internal Reference Redox Reaction , J Electrochem Soc. 168 (2021) 036518. https://doi.org/10.1149/1945-7111/abef4a.

[11] Lin Ru-Shan, Wang You-qun, He Hui, Ye Guo-an, Performance of Ag/AgCl Reference Electrode Packed in Mullite Tube in Molten Chlorides, Journal of Nuclear and Radiochemistry. 41 (2018). https://doi.org/10.7538/hhx.2018.

[12] O. Shirai, T. Nagai, A. Uehara, H. Yamana, Electrochemical properties of the Ag+|Ag and other reference electrodes in the LiCl-KCl eutectic melts, J Alloys Compd. 456 (2008) 498–502. https://doi.org/10.1016/j.jallcom.2007.02.104.

[13] M. Zhang, J. Ge, J. Zhang, L.E. Liu, Redox potential measurement of AgCl in molten LiCl-KCl salt using chronopotentiometry and potentiodynamic scan techniques, Electrochem Commun. 105 (2019). https://doi.org/10.1016/j.elecom.2019.106498.

[14] N.D. Smith, S. Castro Baldivieso, S. Im, H. Kim, Two-Phase Rare-Earth Alloys as Reference Electrodes in Molten Chlorides for Reliable Electrochemical Measurements, in: Minerals, Metals and Materials Series. Rare Earth Metal Technology, 1st ed., Springer Nature Switzerland, (2022): pp. 325–332.

[15] S.C. Baldivieso, N.D. Smith, S. Im, H. Kim, Thermodynamic properties of Gd-Bi alloys determined by emf measurements in LiCl-KCl-$GdCl_3$ electrolyte, J Alloys Compd. 886 (2021) 161229. https://doi.org/10.1016/j.jallcom.2021.161229.

[16] G. Chalyt, P. Bratin, M. Pavlov, A. Kogan, M.J. Perpich, (2004) Voltammetric Reference Electrode Calibration (US Patent No. 6,733,656 B2). U.S. Patent and Trademark Office., 6733656 B2.

[17] J.A. Zamora Zeledón, A. Jackson, M.B. Stevens, G.A. Kamat, T.F. Jaramillo, Methods—A Practical Approach to the Reversible Hydrogen Electrode Scale, J Electrochem Soc. 169 (2022) 066505. https://doi.org/10.1149/1945-7111/ac71d1.

[18] M. Iizuka, Diffusion Coefficients of Cerium and Gadolinium in Molten LiCl-KCl, J Electrochem Soc. 145 (1998) 84–88. https://doi.org/10.1149/1.1838216.

[19] F. Lantelme, Y. Berghoute, Electrochemical Studies of $LaCl_3$ and $GdCl_3$ Dissolved in Fused LiCl-KCl, J Electrochem Soc. 146 (1999) 4137–4144. https://doi.org/10.1149/1.1392604.

[20] P. Delahay, Talivaldis; Berzins, Oscillographic Polarographic Waves for the Reversible Deposition of Metals on Solid Electrodes, J. Am. Chem. Soc. 75 (1952) 555–559.

[21] M.M. Tylka, J.L. Willit, J. Prakash, M.A. Williamson, Method Development for Quantitative Analysis of Actinides in Molten Salts, J Electrochem Soc. 162 (2015) H625–H633. https://doi.org/10.1149/2.0401509jes.

[22] G.J. Janz, C.B. Allen, N.P. Bansal, R.M. Murphy, R.P.T. Tomkins, Physical properties data compilations relevant to energy storage :, Gaithersburg, MD, (1979). https://doi.org/10.6028/NBS.NSRDS.61p2.

[23] G.J. Janz, Thermodynamic and Transport Properties for Molten Salts, Physical and Chemical Reference Data. 17 (1988).

[24] A.J. Bard, L.R. Faulkner, Electrochemical Methods: Fundamentals and Applications, 2nd Edition, Wiley, Chapter 6. 239-252 (2000).